Supporting Information

Efficient Photo-Driven Ion Pump through Slightly Reduced Vertical Graphene Oxide Membranes

Xinyi Du,[a] Junchao Liu,[b] Zhitong Han,[a] Jiansheng Chen,[a] Lina Wang,[c] Xinyi Zhang,[a] Yue Guo,[a] Xuran Liu,[d] Jinming Zhou,[a,] and Pan Jia[a,]**

[a] Hebei Key Laboratory of Inorganic Nanomaterials, College of Chemistry and Material Science, Hebei Normal University, Shijiazhuang 050024, P. R. China

[b] School of Sciences, Xi'an University of Technology, Xi'an 710048, P. R. China

[c] Testing and Analysis Center, Hebei Normal University, Shijiazhuang 050024, P. R. China

[d] College of Material Engineering, North China Institute of aerospace engineering, Langfang, 065000, P. R. China

*Corresponding author

Email: zhoujm@iccas.ac.cn (J. Zhou), jiapan15@mails.ucas.ac.cn (P. Jia)

Table of Content:

1. Characterization of GO

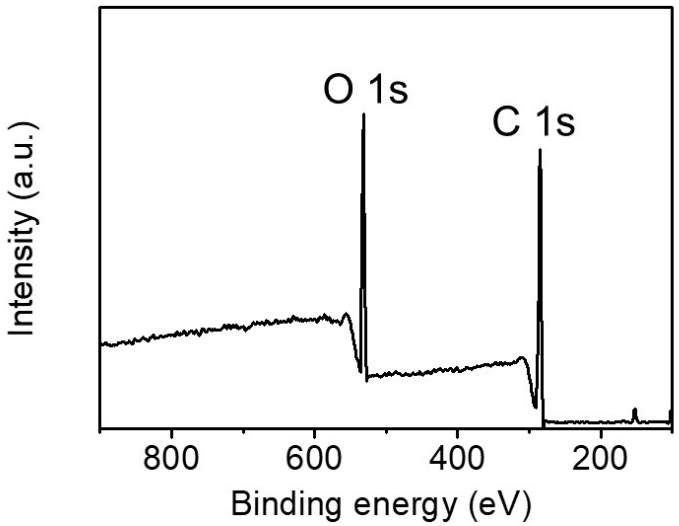

Fig. S1 XPS survey spectrum of GO, suggesting an oxygen atomic ratio of 24%.

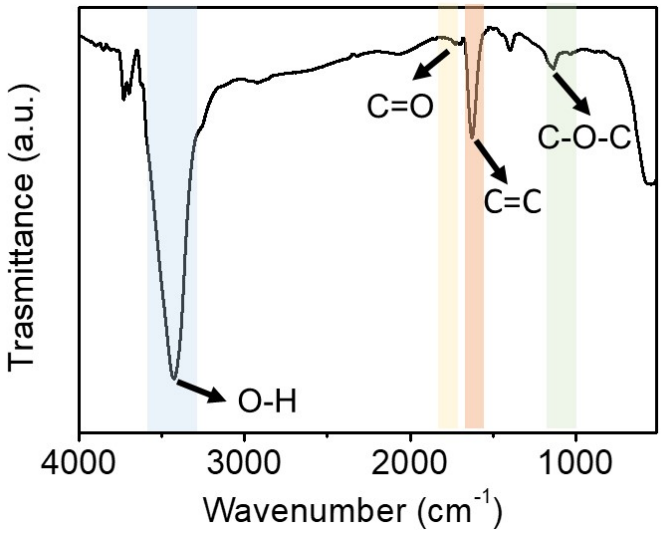

Fig. S2 FTIR spectrum of GO. The absorptions at 3400 cm^{-1}, 1720 cm^{-1}, 1618cm^{-1}, and 1077 cm^{-1} ascribe to stretching vibration of -OH, C=O, C=C, and C-O-C, respectively.

2. Stability of GOM in water

Although the GOM is hydrophilic, it can keep intact in water for at least one week owing to the thermal annealing process.[1]

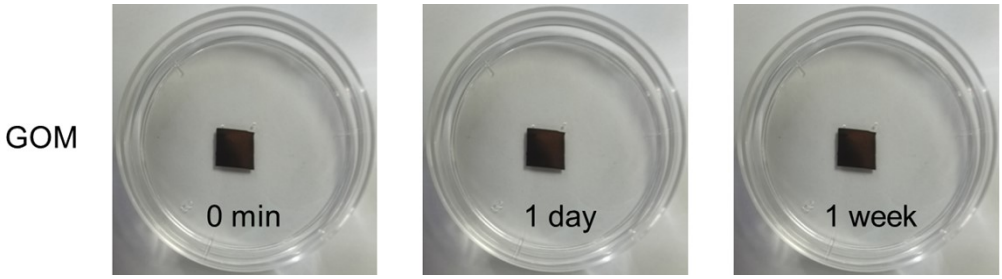

Fig. S3 Stability of GOM in water. The GOM can keep intact in water for more than one week.

3. Characterization of GOM

The Raman spectroscopic study of GOM was conducted using a 532 nm laser. The main characteristics of the Raman spectrum are the G and D peaks, which occur at 1599 cm^{-1} and 1347 cm^{-1}, respectively. The G band originates from the in-plane vibration of the sp^2 domain, while the D band arises from the breathing mode of aromatic rings with defects.[2] The Raman spectrum shows similar intensities for the G and D peaks (Fig. S4), indicating an equivalent of sp^2 and sp^3 carbons.

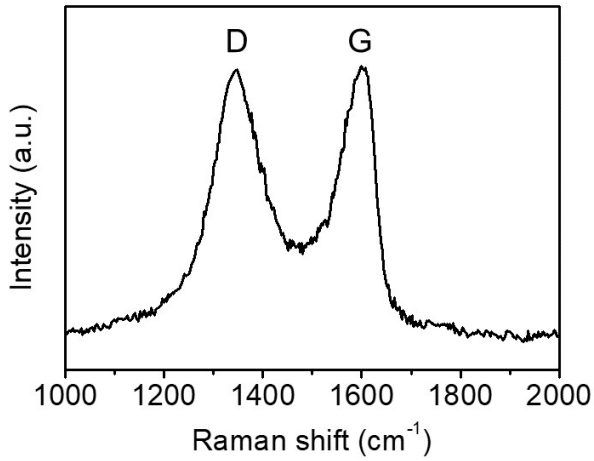

Fig. S4 Raman spectrum of GOM.

To determine the bandgap of GOM, we tested the absorbance spectrum of GO (Fig. S5a). The peaks near 230 nm and 300 nm are attributed to π-π* transitions of C=C and n-π* transitions of C=O, respectively.[3] The square of the absorption energy (αhν, where α is the absorbance) against the photon energy (E) is plotted to determine the energy value for the bandgap. As depicted in Fig. S5b, the converted Tauc plots do not show sharp adsorption edges for well-define E_g, due to the varying oxidation levels of graphene.[4] Based on approximate linear extrapolation, Fig. S5b gives bandgap energy values of 2.8–3.8 eV.

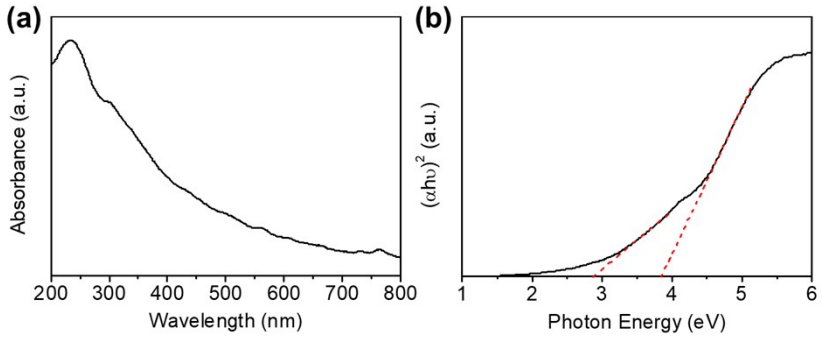

Fig. S5 Bandgap determination of GO. (a) UV-vis spectrum of GO. (b) Tauc plot of GO.

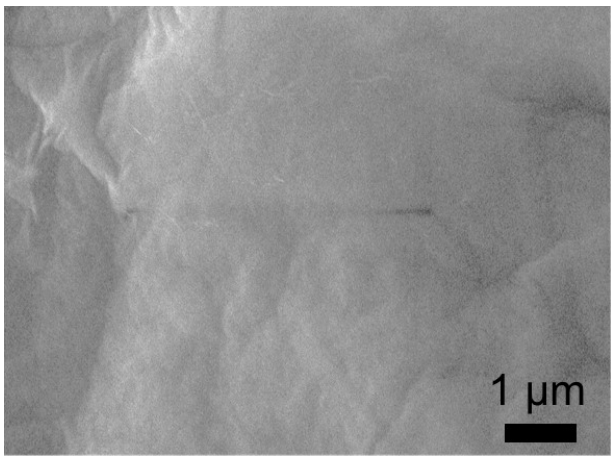

Fig. S6 SEM observation on the surface of the GOM shows smooth surface morphology.

4. Cation transference number

In the presence of a transmembrane concentration difference, we employed agar-saturated potassium chloride salt bridges to eliminate the imbalanced redox potential at the electrode|electrolyte interface. We recorded the current-voltage response using Ag/AgCl electrodes and a Keithley 6487 source meter from Keithley Instruments. To assess the diffusion potentials, measurements were conducted under various concentration gradients ranging from 10 to 100-fold. The electrolyte used in all of these tests was KCl.

To quantify selective ion transport, the cation transference number (t_+) serves as a crucial metric. Calculating the value of t_+ is achieved using the following formula:[5]

$$2t_+ - 1 = \frac{E_{Diff}}{\frac{RT}{zF} ln(\frac{\gamma_{C_H} C_H}{\gamma_{C_L} C_L})} \quad \text{(S1)}$$

In this equation, several key parameters are involved: R denotes the ideal gas constant, T represents temperature, z stands for the charge valency, F denotes the Faraday constant, γ represents the activity coefficient of ions, while C_H and C_L refer to the high and low ion concentrations, respectively. Notably, the measured t_+ value exceeds 0.79, indicating a high level of cation-selectivity (as depicted in Fig. S7). A comprehensive summary of these results can be found in Tab. S1.

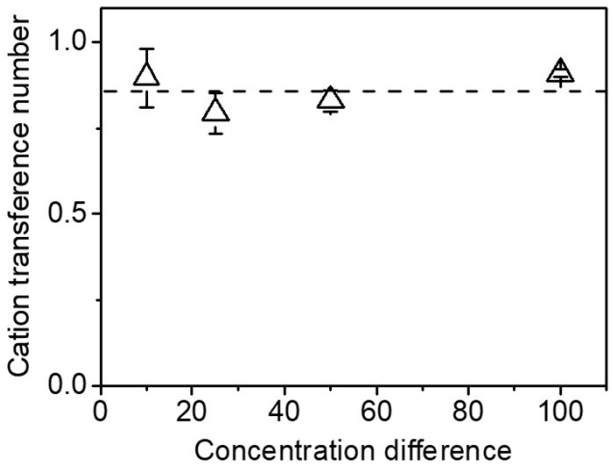

Fig. S7 Cation transference number (t_+) measured under varied concentration gradients.

Tab. S1 Summary of the activity coefficient (γ), diffusion potential, and cation transference number (t_+).

Concentration difference (M/M)	γ	Diffusion potential (mV)	t_+
$10^{-6}/10^{-5}$	0.999/0.996	46.9±4.5	0.89±0.08
$10^{-6}/2.5\times10^{-5}$	0.999/0.994	48.4±3.6	0.79±0.06
$10^{-6}/5\times10^{-5}$	0.999/0.992	66.3±2.4	0.83±0.03
$10^{-6}/10^{-4}$	0.999/0.989	97.0±1.2	0.91±0.01

5. Effect of H^+ and OH^- for ionic conductance

We also investigated the influence of H^+ and OH^- ions on ionic conductance. Initially, we conducted tests to measure the *I-V* curves in an electrolyte solution containing 10^{-6} M KCl, both with and without GOM (Fig. S8). The ionic conductance was determined to be 0.23 μS with GOM and 0.047 μS without GOM. Additionally, we assessed the conductance in deionized (DI) water, both with and without GOM, resulting in conductance values of 0.094 μS and 0.038 μS, respectively. The disparity in ionic conductance between the presence and absence of GOM is attributed to the $G_{surface}$. Furthermore, in the absence of GOM, we observed that the ionic conductance of the bulk 10^{-6} M KCl was slightly higher than that of DI water, indicating a significant contribution of H^+ and OH^- ions to the G_{bulk} in the low concentration region. This is due to the higher diffusivity of H^+ and OH^- ions compared to K^+ and Cl^- ions (Tab. S2). These results suggest that deviations in conductance from the bulk are primarily caused by $G_{surface}$, while deviations from the linear relationship are influenced by both surface-charge-governed ion transport and the effects of H^+ and OH^- ions.

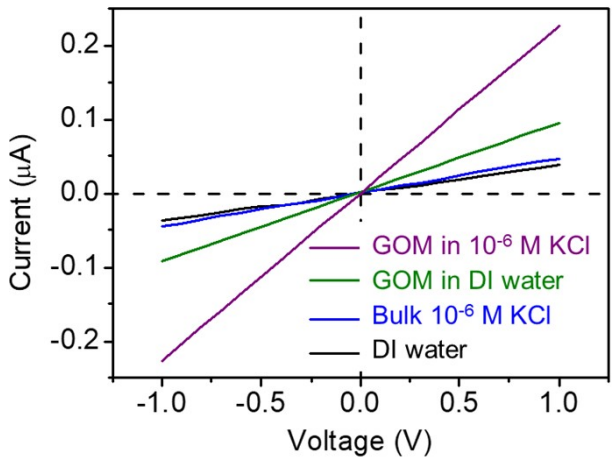

Fig. S8 *I-V* curves for GOM in 10^{-6} M KCl and DI water, as well as for the bulk 10^{-6} M KCl and DI water.

Tab. S2 Ionic mobility and diffusion coefficient in water.

Ion	Mobility[6] (u, 10^{-8} m^2 s^{-1} V^{-1})	Diffusion coefficient[7] (10^{-9} m^2 s^{-1})

K^+	7.62	1.96
Cl^-	7.92	2.03
H^+	36.20	9.31
OH^-	20.50	5.27

6. Long-term stability of photocurrent

We examined the stability of the photocurrent during prolonged exposure to light. A representative result is displayed in Fig. S9. Notably, the photocurrent remained stable for a duration exceeding 500 s.

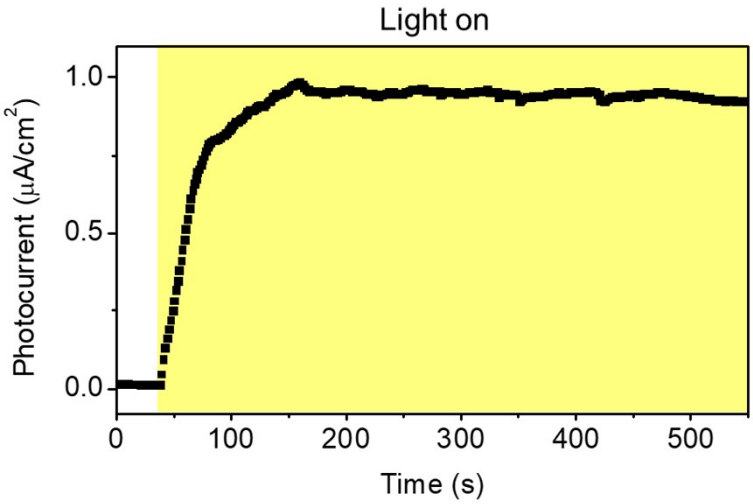

Fig. S9 Ionic photocurrent generation under continuous illumination. The light intensity was 133 mW cm^{-2}. The electrolyte was 10^{-4} M KCl solution.

7. Time constant

We conducted an assessment of the equilibrium time for the GOM. Typical photocurrent-time curves were shown in Fig. S9. To quantify the time constant of the current trace, we applied a fitting procedure to the experimental data using an exponential function,[8]

$$I = I_0 - Aexp(-\frac{t}{\tau}) \quad \text{(S2)}$$

Here, τ represents the time constant, while I_0 and A serve as the fitting parameters. When subjected to a light intensity of 133 mW/cm^2, the time constant for the current trace depicted in Fig. S10 was approximately 25.88 seconds.

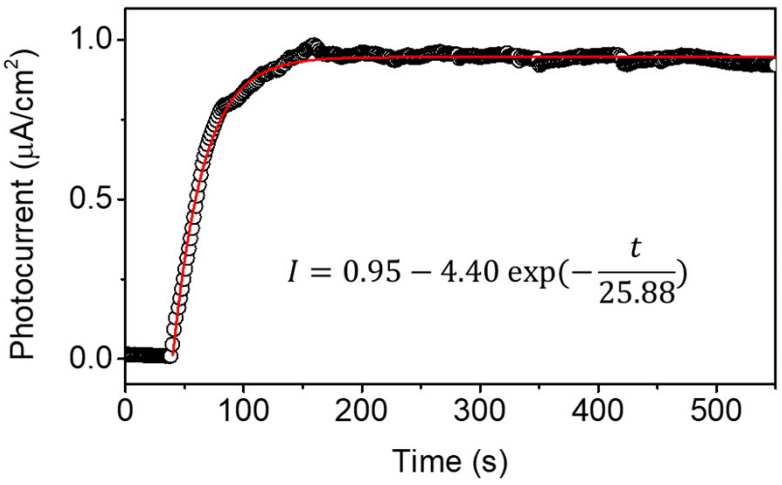

Fig. S10 The photocurrent-time curves can be numerically fitted with an exponential function. The black circles were experimental data and the red lines were fitting curves.

8. Temperature effect

To investigate the possibility of photo-induced thermal effects influencing our observations, we initiated a comprehensive investigation. Firstly, we utilized a handheld infrared camera (HIKMICRO H16) to monitor temperature fluctuations on the GOM surface during light illumination. As depicted in Fig. S11a, the GOM exhibited a noticeable increase in temperature when subjected to light, relative to its immediate surroundings. The temperature increase exhibited a positive correlation with both light intensity and illumination time. Under typical light conditions with an intensity of 133 mW cm^{-2}, the temperature rise did not exceed 22 ^{o}C after 30 s of light illumination.

Under these conditions, we conducted ionic current measurements at elevated temperatures by directly heating the ionic solution within one reservoir, simulating the effects of light-induced thermal changes. We maintained the temperature increment at approximately 30 ^{o}C, while keeping all other experimental parameters consistent with those outlined in the main text. Fig. S11c illustrates that, in the presence of elevated temperature on one side, only a minimal change in ionic current was observed in the GOM. In stark contrast, the ionic current change induced by light illumination exceeded 8 times the magnitude of the thermal-induced effect.

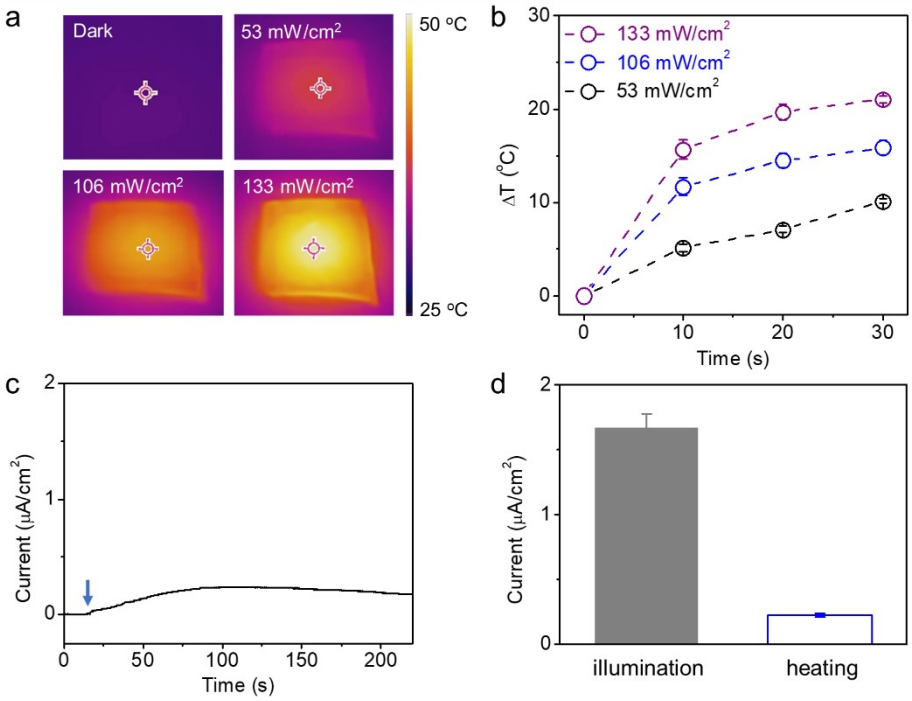

Fig. S11 Temperature effect. (a) Thermal images of the GOM before and after 30 seconds of light illumination. The light intensities used were 53, 106, and 133 mW cm^{-2}, respectively. (b) Temperature increase (ΔT) as a function of illumination time at different light intensities. Error bars represent standard deviation. (c) Time traces of ionic current during the heating process. The arrow indicates the point at which the temperature change occurred in the reservoir. (d) Comparison of the change in ionic current induced by light illumination (solid) and temperature rise (hollow). Illumination and heating were applied to the left side of the GOM. The electrolyte solution used was 10^{-3} M KCl.

9. Ionic current time trace as a function of electrolyte concentration

As the electrolyte concentration increases, the photo response enhances due to the increasing number of ions.[9]

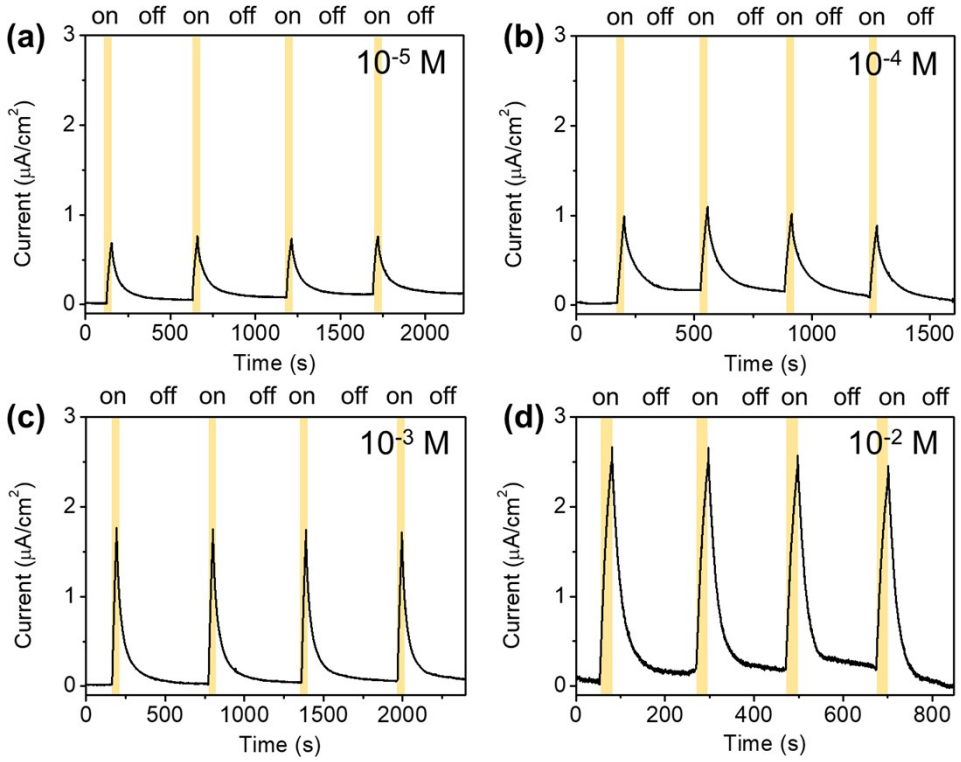

Fig. S12 Ionic photocurrents of a variety of electrolyte concentrations. The light intensity was 133 mW cm^{-2}, and the duration of each light illumination was consistently set at 30 s.

10. Incident-photon-to-current efficiency (IPCE)

The IPCE was calculated using the equation,[10, 11]

$$IPCE(\%) = \frac{1240 \times I_{ph}(mA/cm^2)}{P_L(mW/cm^2) \times \lambda(nm)} \times 100 \quad \text{(S3)}$$

where I_{ph} is the photocurrent density, and P_L is the incident light power at a specific wavelength (λ). The ICPE was calculated using the data from Fig. 4a. The light intensity was 133 mW cm^{-2}. As the electrolyte concentration increased from 10^{-5} to 10^{-2} M, the performance of the ICPE steadily improved (Fig. S13).

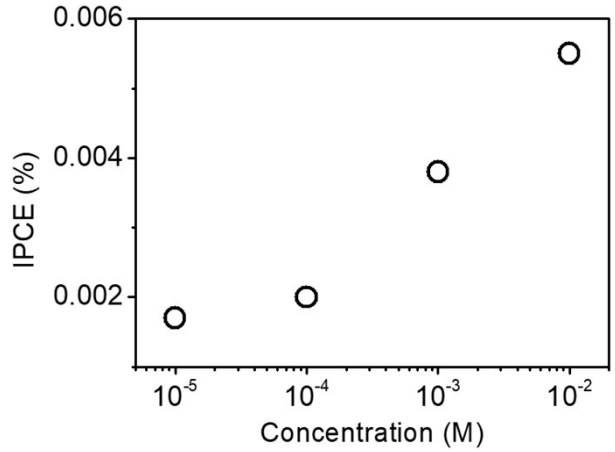

Fig. S13 IPCE of GOM as a function of electrolyte concentration from 10^{-5} to 10^{-2} M. The light intensity was 133 mW cm^{-2}. The wavelength was centered at 405 nm.

11. Ionic current time trace as a function of light intensity

The magnitude of the ionic photocurrent increases with the light intensity, due to the enhanced light-induced transmembrane electric potential [12].

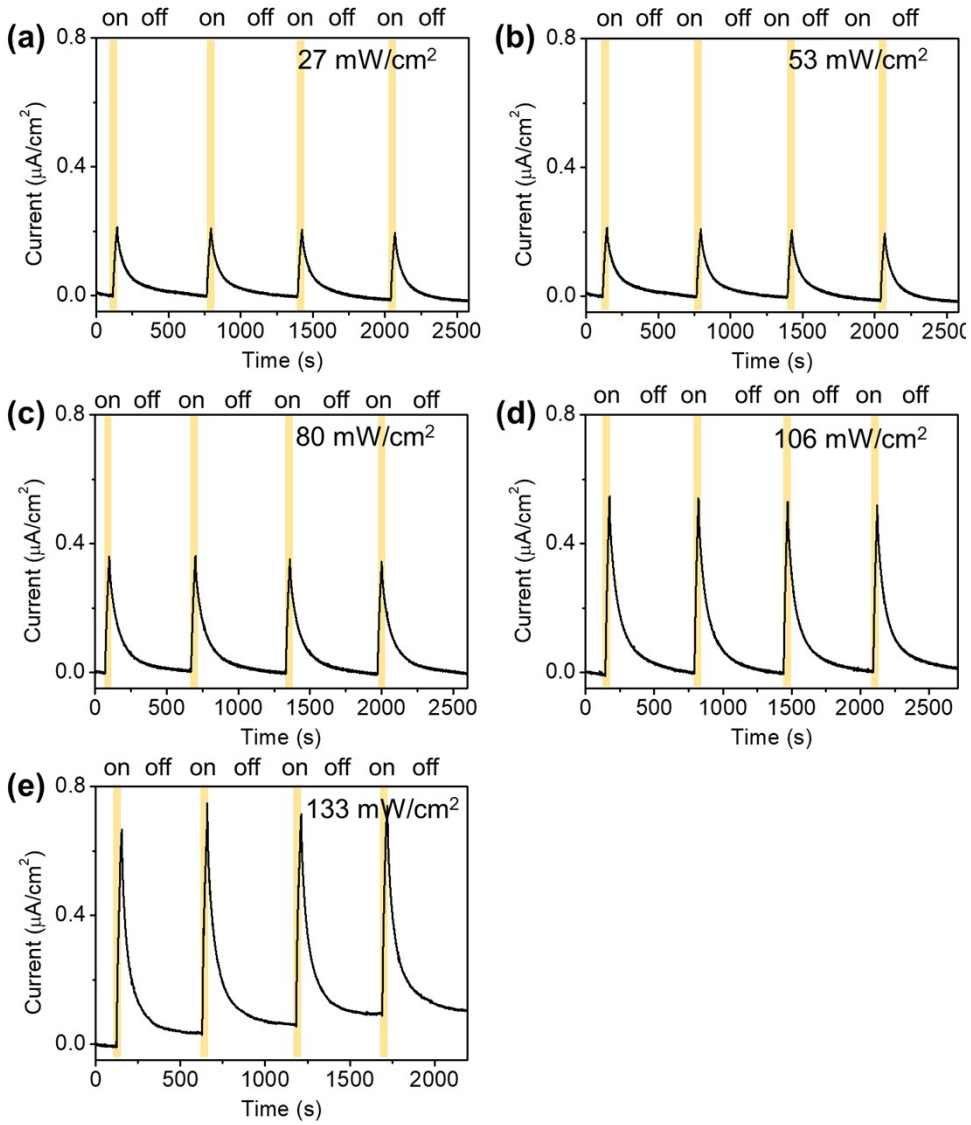

Fig. S14 Ionic photocurrents of a variety of light intensities. The electrolyte solution was 10^{-5} M KCl, and the duration of each light illumination was consistently set at 30 s.

12. Photoresponsivity

The photoresponsivity (R) can be calculated using the data from Fig. 4b with the formula,[12]

$$R = \frac{I_{ph}}{P_L} \tag{S4}$$

Here, I_{ph} represents the photocurrent, and P_L denotes the incident light power. Notably, the average photoresponsivity for GOMs was found to be 4.45 ± 0.62 μA/W, as illustrated in Fig. S15.

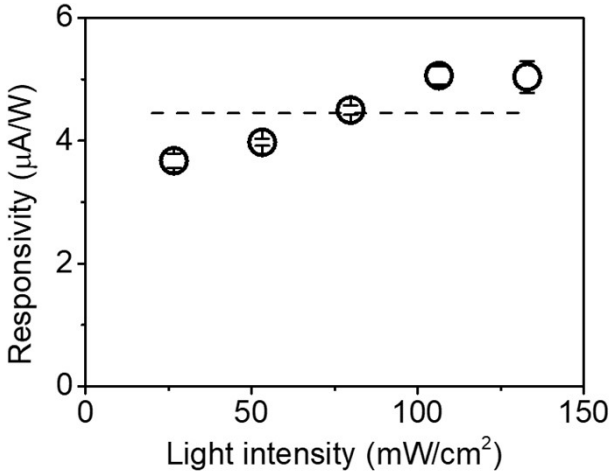

Fig. S15 Photoresponsivity of GOM.

13. References

1. J. Ji, Q. Kang, Y. Zhou, Y. Feng, X. Chen, J. Yuan, W. Guo, Y. Wei and L. Jiang, *Adv. Funct. Mater.*, 2017, **27**, 1603623.

2. G. Eda and M. Chhowalla, *Adv. Mater.*, 2010, **22**, 2392-2415.

3. K. P. Loh, Q. Bao, G. Eda and M. Chhowalla, *Nat. Chem.*, 2010, **2**, 1015-1024.

4. T.-F. Yeh, J.-M. Syu, C. Cheng, T.-H. Chang and H. Teng, *Adv. Funct. Mater.*, 2010, **20**, 2255-2262.

5. J. Gao, W. Guo, D. Feng, H. Wang, D. Zhao and L. Jiang, *J. Am. Chem. Soc.*, 2014, **136**, 12265-12272.

6. K. J. Laidler and J. H. Meiser, *Boston: Houghton Mifflin*, 1999, 274.

7. P. Vanýsek, *CRC Press*, 1992, (5-111)-(115-113).

8. S.-C. Kung, W. E. van der Veer, F. Yang, K. C. Donavan and R. M. Penner, *Nano Lett.*, 2010, **10**, 1481-1485.

9. P. Jia, L. Wang, Y. Zhang, Y. Yang, X. Jin, M. Zhou, D. Quan, M. Jia, L. Cao, R. Long, L. Jiang and W. Guo, *Adv. Mater.*, 2021, **33**, 2007529.

10. S. Seo, S. Kim, H. Choi, J. Lee, H. Yoon, G. Piao, J. C. Park, Y. Jung, J. Song, S. Y. Jeong, H. Park and S. Lee, *Adv. Sci.*, 2019, **6**, 1900301.

11. Q. Zhang, Q. Liang, D. K. Nandakumar, S. K. Ravi, H. Qu, L. Suresh, X. Zhang, Y. Zhang, L. Yang, A. T. S. Wee and S. C. Tan, *Energy Environ. Sci.*, 2020, **13**, 2404-2413.

12. P. Jia, Q. Wen, D. Liu, M. Zhou, X. Y. Jin, L. P. Ding, H. L. Dong, D. N. Lu, L. Jiang and W. Guo, *Small*, 2019, **15**, 1905355.